

www.acsanm.org Article

Rapid Photothermal Healing of Vitrimer Nanocomposites Activated by Gold-Nanoparticle-Coated Graphene Nanoplatelets

Yixin Ren,[○] Amber M. Hubbard,[○] Drake Austin, Jinghang Dai, Chen Li, Renjiu Hu, Peter Papaioannou, Catalin R. Picu, Dominik Konkolewicz, Alireza Sarvestani, Nicholas Glavin, Vikas Varshney, Ajit K. Roy, Zhiting Tian, and Dhriti Nepal*



Cite This: ACS Appl. Nano Mater. 2024, 7, 18769-18778



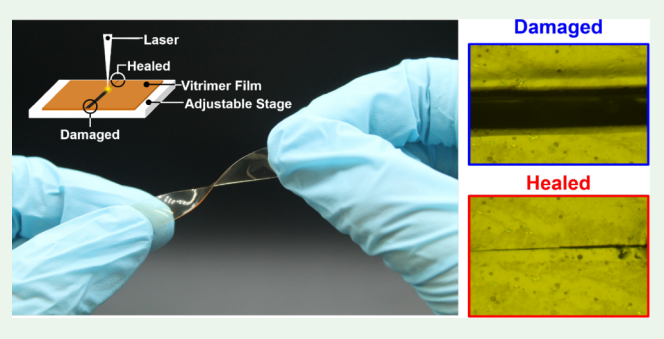
ACCESS

Metrics & More

Article Recommendations

Supporting Information

ABSTRACT: Vitrimers, an emerging class of polymer materials, are thermosets with dynamic covalent cross-linkers, allowing for topology rearrangement at elevated temperatures. However, vitrimers have several drawbacks, such as slow response times and often lack photothermal catalytic activity. Herein, we demonstrate that embedding functional nanofillers, i.e., hierarchically assembled plasmonic gold nanoparticles (AuNPs) on graphene nanoplatelets (GNPIs) into a vitrimer matrix, induces an ultrafast photothermal healing response. Unlike previous research that mainly focused on bulk materials, our exploration of vitrimer nanocomposite films uncovers unique advantages, such



as optical transparency in the visible wavelength, flexibility, and ultrafast localized healing upon exposure to a 532 nm wavelength laser. These remarkable properties of vitrimer nanocomposite films were demonstrated with three various filler compositions and concentrations, where AuNPs/GNPls serve as a powerful filler. Photothermally activated self-healing of these hybrid materials is demonstrated by taking advantage of the localized surface plasmon resonance (LSPR) of AuNPs and the broad absorbance wavelength and high thermal conductivity of GNPls. Furthermore, profilometry is utilized to quantify the volume percent recovery of healing, providing quantitative evidence of increased healing with a higher filler concentration and laser dosage. This localized, ultrafast healing is pivotal for future coating applications, where bulk heating could lead to undesirable deformations. Our comprehensive understanding of the role of filler composition, filler concentration, and laser dosage in the self-healing properties of films opens up a wide array of potential applications for these light-responsive functional materials. The potential applications of these materials span from self-healing coatings to flexible electronics, inspiring a new era of innovative solutions.

KEYWORDS: vitrimer, photothermal response, self-healing, laser, nanocomposite, film

INTRODUCTION

Epoxy-based thermosets have garnered significant interest in numerous applications, spanning from electronics to structural composites. This interest is mainly due to their unique properties, including excellent thermal stability, adhesive strength, and ease of processing. However, these materials are also typically brittle and difficult to repair due to their permanently cross-linked network. Vitrimers are an emerging class of cross-linked thermoset polymers that exhibit dynamic covalent bond exchange reactions at elevated temperatures, enabling polymer materials to reform and reshape like thermoplastics while maintaining the mechanical performance of traditional epoxy resin.²⁻⁴ Various associative dynamic exchange reactions have been introduced where bond-breaking and bond-forming occur simultaneously, retaining solid-like properties throughout the dynamic exchange process. These exchange reactions include transesterification, dioxaborolane, vinylogous urethane, disulfide, imine, silyl ether, and transamination, and others, enabling desirable reforming and selfhealing capabilities at temperatures above their topology freezing temperature $(T_{\rm v})^{.5,6}$

The dynamic covalent bond exchange reactions in epoxy vitrimers provide beneficial properties, but they are typically initiated thermally, making it challenging to repair damaged parts or devices during use. Heating the material in bulk rather than at the specific damaged site results in inefficient energy usage due to excessive heat application, ultimately increasing the overall repair cost. In addition, bulk heating methods can have detrimental outcomes (e.g., thermal expansion, delamination, and deformation, etc.), 7 making it challenging to repair

Received: April 15, 2024
Revised: July 18, 2024
Accepted: July 24, 2024
Published: August 2, 2024





confined damage, such as cracks and scratches. Herein, we report an alternative, photothermally activated healing method that allows localized heating of damaged epoxy materials with ultrafast healing via nanofiller addition.

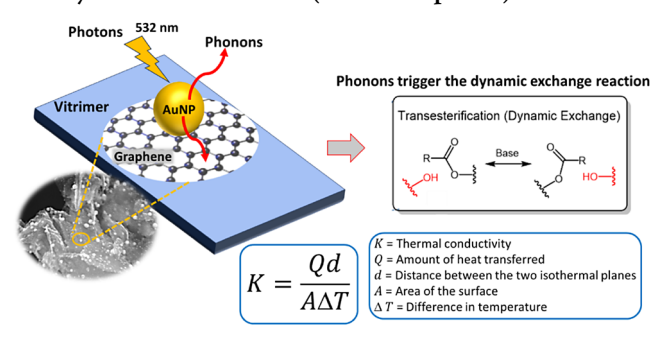
While most vitrimer studies explore bulk properties,8,9 vitrimer thin film mechanics and self-healing properties are poorly understood. 9,10 This underexplored research topic is of significant interest for healable and reconfigurable coatings and adhesives. 11 In general, the addition of nanofillers enhances the mechanical and thermal performance of bulk nanocomposites and further increases the application space. Specifically, the addition of light-absorbing nanofiller to the vitrimer network is highly promising because photothermal heating and damage repair are possible via localized photon-phonon conversion. 10,12 Previous studies have shown promising photothermal effects using gold nanoparticles, ¹³ gold nanorods, ¹⁰ graphene, ¹² and iron nanoparticles. ¹⁴ The fundamental mechanism for achieving efficient healing lies in the realm of the high light absorption properties and thermal conductivity of these nanoparticles. By strategically designing hybrid nanomaterials with these attributes, we can potentially unlock a more synergistic effect.

Generating films with a uniform nanofiller dispersion is one of the most critical steps to achieving these goals. Despite significant interest, uniform filler dispersion in a thermoset epoxy composite remains a substantial challenge for these materials. 15,16 Previous studies have explored the impact of filler dispersion upon T_{v} in bulk vitrimer composites; therefore, the temperature at which these composite films could be reconfigured and healed.¹⁷ Our group has previously reported the synthesis of graphene nanoplatelets decorated with gold nanoparticles¹⁸ via spontaneous reduction of gold acetate on graphene platelets.¹⁸ Here, defects on the graphene surface trigger the nucleation of Au acetate reduction, and with Ostwald ripening, it grows as a nanoparticle. 18 As a result, the anchored AuNPs appeared as a patchy coating rather than full coverage. From here on, the gold-coated graphene is termed AuNPs/GNPIs. For this thin film study, we have found these AuNPs/GNPls are ideal fillers as the graphene platelets have an exceptionally high thermal conductivity¹⁹ and both AuNPs and GNPIs can absorb light in the visible spectrum. 18 Upon illumination with a 532 nm laser (Scheme 1), the AuNPs exhibit localized surface plasmon resonance, allowing them to undergo photothermal conversion. Due to graphene's very high thermal conductivity and its relatively large area, this localized heat is more efficiently transferred into the vitrimer. This localized heat triggers a dynamic transesterification reaction in the presence of a base catalyst.

Photothermally activated healing is of particular interest for in-service part maintenance where compression molding, a literature standard for vitrimer healing, is not industrially relevant. This is particularly important, as the part requiring maintenance increases in shape complexity. Furthermore, while previous studies have demonstrated that the bulk healing of vitrimers can take on the order of minutes to hours, ^{20–22} the photothermal conversion of the AuNPs/GNPls is less than one second. This ultrafast response time that has been quantitatively validated is unmatched for vitrimer composites, to the best of the author's knowledge.

Herein, we report the production of vitrimer films and vitrimer nanocomposite films for self-healing and reconfigurable coatings with a range of nanofiller compositions and concentrations. These vitrimer nanocomposites exhibit in-

Scheme 1. A Schematic Representation of Photo-Thermal Conversion. AuNP Coated on Graphene Nanoplatelet on Top of a Vitrimer Matrix, with the Left Side Demonstrating 532 nm Laser Illumination (Localized Surface Plasmon Resonance of AuNP), Converting the Photons to Phonons Locally due to Absorbance (Heat Dissipation)^a



"Due to its very high thermal conductivity (K), Graphene transfers high heat (Q), passing it to the Vitrimer. This localized heat triggers a dynamic transesterification reaction in the presence of a base catalyst, as shown on the right.

creasing $T_{\rm v}$ values with increasing filler concentration, improved stiffness, increased absorption, and ultrafast self-healing via efficient photothermal conversion. In addition, we demonstrate that increasing the filler concentration and laser dosage leads to improved healing efficiencies of vitrimer nanocomposite films, where localized heating of the filler is confirmed by molecular dynamic simulations. These light-responsive smart vitrimer nanocomposite thin films with high healing efficiencies have excellent potential as coatings for a range of industrial applications.

RESULTS AND DISCUSSION

All vitrimer films are produced using a previously reported chemistry (cf. Scheme S1), where the dynamic covalent bond exchange reaction, which dominates at $T > T_{\rm v}$, is a transesterification reaction. Fourier-transform infrared spectroscopy (FTIR) was performed on both the fabricated vitrimer films and the epoxy prepolymer (cf. Figure S1), ensuring complete curing. While only one epoxy vitrimer is explored throughout this work, the nanofiller composition and concentration are varied to explore its impact on photothermal healing.

Thin Film Production and Characterization. Vitrimer synthesis procedures are outlined in the Materials and Methods section and are schematically depicted in Figure S2. For vitrimer nanocomposite films, it was crucial to ensure well-dispersed nanofillers, requiring additional shear mixing and sonication of the nanofillers into the epoxy prepolymer. Figure S3 demonstrates the excellent dispersion quality achieved with an increased level of nanofiller mixing.

Throughout this work, three different nanofiller compositions are explored: Graphene nanoplatelets (GNPIs), Gold nanoparticles (AuNPs), and AuNPs/GNPIs. In addition, the nanofiller concentration is varied from 0 to 0.5 wt %. Figure 1a shows a neat vitrimer film (i.e., no nanofiller), which is transparent and flexible. However, this flexibility also indicates a lack of stiffness, as seen in Figure 1b, where the vitrimer film bends under its own weight, but can easily be twisted into a loop. In contrast, with the nanofiller addition, the vitrimer nanocomposite film becomes increasingly stiff and no longer

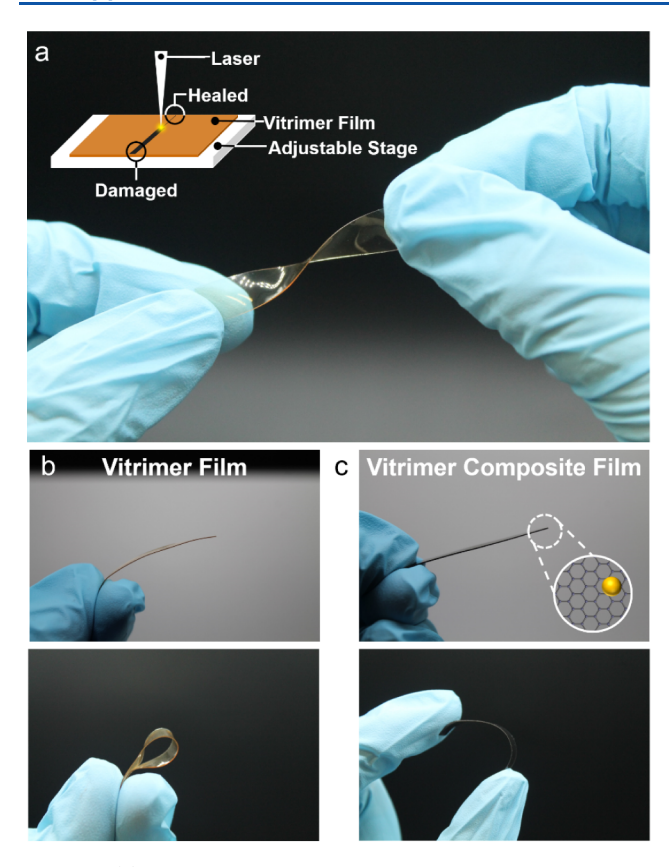


Figure 1. (a) Vitrimer films are twisted to show the transparency and flexibility of these materials. A schematic diagram also shows the ability to heal damaged vitrimer films with laser irradiation. (b) A neat vitrimer film is held and bent to show the flexibility of these materials. These neat vitrimer films have an average thickness of 0.209 ± 0.044 mm. (c) A vitrimer nanocomposite film is held to show the increased rigidity with filler addition; the filler in this case is 0.5 wt % AuNPs/GNPs, where the sample thickness is 0.212 ± 0.043 mm.

flexes readily (Figure 1c). These films are of comparable thicknesses, so the added stiffness is attributed to the filler addition. As previously noted, and schematically shown in Figure 1a, the primary goal of this research is to heal damaged vitrimer films via photothermal heating, which we will demonstrate is only possible via nanofiller incorporation.

As expected, the transparency of these vitrimer films decreases with nanofiller addition. Figure 2a visually shows the vitrimer films when placed over a sheet of paper displaying



Figure 2. (a) Sample photographs of vitrimer and vitrimer nanocomposite films where the filler composition and concentration are noted above the image. All the films are placed over a printed U.S. Air Force logo to demonstrate a decrease in transparency with added filler. (b) Optical microscopy is shown for all the films where a good filler dispersion is demonstrated.

the U.S. Air Force logo, where the filler is specified above the photograph. As expected, the transparency decreases with the filler addition due to the dark color of the filler. In addition, optical microscopy (cf. Figure 2b) shows the high dispersion quality of these vitrimer nanocomposites.

Figure 3a shows a representative TEM image of a AuNPs/GNPls powder before mixing it with the vitrimer. The image

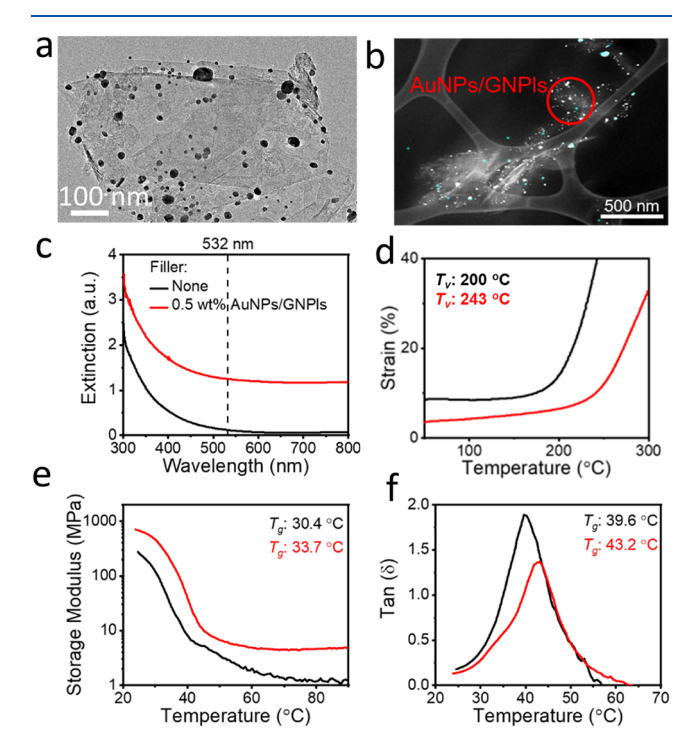


Figure 3. High resolution TEM image of (a) AuNPs/GNPls powder before mixing it with vitrimer, showing random distribution of AuNP adhered to GNPIs. (b) High-angle annular dark-field scanning-transmission electron microscope (HAADF-STEM) with energy-dispersive X-ray spectroscopy (EDX) image of a vitrimer nano-composite film (microtomed) with 0.5 wt % AuNPs/GNPls filler. Comparing a neat vitrimer film (black) to a vitrimer nanocomposite film with 0.5 wt % AuNPs/GNPls filler (red), results are shown of (c) UV—visible spectroscopy (UV—vis), (d) nonisothermal creep via dynamic mechanical analysis (DMA), and DMA temperature sweep (e) storage modulus and (f) tan δ .

shows spherical AuNPs (black particles) of different sizes (~5 nm to <50 nm) randomly adhered to GNPls (gray sheets). As reported in our prior work, 18 the sizes and distribution of the AuNPs are highly dependent on the concentration and processing conditions. However, visualizing these nanofillers in our nanocomposite films from electron microscopy imaging is nontrivial due to the poor electron contrast of graphene and polymer, and the overall low percentage of AuNPs in the system. Figure 3b shows HAADF-STEM with EDX mapping of 0.5 wt % AuNPs/GNPls vitrimer film, where the samples are sliced to <100 nm thin film via cryo-microtome. In the TEM image, it is hard to distinguish graphene within the polymer film. This is due to both graphene and polymers containing carbon atoms, which results in comparable contrast levels when imaged using TEM. Additionally, the arrangement and overlapping of graphene layers within the polymer matrix further hinder the distinction between the two. Nevertheless, the gold is identified with a cyan coloring, confirming the

presence of AuNPs in the nanocomposite with additional images on elemental mapping in Figure S4.

Furthermore, we chose to characterize the difference between neat vitrimer films and vitrimer nanocomposite films (i.e., 0.5 wt % AuNPs/GNPls) with various techniques (cf. Figure 3c-f). A key aspect of this work is taking advantage of the improved photothermal responsiveness provided via filler incorporation. Figure 3c confirms an increase in absorption, e.g., extinction, at 532 nm wavelength. Additional UV—vis spectra are provided in Figures S5,S6. We should note that for samples with only AuNPs present as a filler material, the expected localized surface plasmon resonance (LSPR) peak around 540 nm is evident; however, this peak is not apparent in Figure 3c, where the presence of GNPls dominates the broad absorption in the spectra.

While this study aims to explore the photothermal self-healing of vitrimer films, this response requires a complete understanding of how filler addition impacts the thermomechanical properties of the resulting nanocomposites. Figure S7 explores the impact of filler addition upon the nanocomposite's thermal degradation. For example, while a neat vitrimer film reaches a degradation temperature ($T_{\rm 5\%}$) at 343 °C, this value minimally increases to 355 °C for a sample with a 0.5 wt % concentration of AuNPs/GNPls. This trend is critical, as the $T_{\rm 5\%}$ will be treated as the maximum operating temperature for all samples moving forward and discussed in detail later.

In addition to $T_{5\%}$, it is also critical to understand the glass transition temperature $(T_{\rm g})$ and $T_{\rm v}$ of these materials. While $T_{\rm g}$ identifies the temperature where these materials are rubbery, $T_{\rm v}$ identifies the temperature where the dynamic covalent bond exchange reaction dominates, allowing for self-healing. Figure S8 demonstrates that the $T_{\rm g}$ increases minimally from 32 to 35 °C with filler addition via differential scanning calorimetry (DSC). Results from the temperature sweep experiments via dynamic mechanical analysis (DMA) validate this increase in $T_{\rm g}$ with filler addition, as seen in Figure 3e,f and as previously reported in literature. Additional temperature sweep results are seen for all the filler compositions and concentrations in Figure S9.

Finally, we demonstrate an increase in the nanocomposite $T_{\rm v}$ value with filler addition as measured via nonisothermal creep experiments (cf. Figure 3d). The $T_{\rm v}$ is measured as the intersection between the pseudohorizontal and pseudovertical regions of the strain—temperature curve, ²³ where there is a clear increase in $T_{\rm v}$ with filler addition (cf. Figure S10). This trend has been previously reported for vitrimer nanocomposites on a bulk scale, and is confirmed here for nanocomposite films. ¹⁷ The increase in the $T_{\rm v}$ is possible due to multiple factors, such as hindered network rearrangement due to filler and increased catalyst heterogeneity. Also, this increased $T_{\rm v}$ confirms the desired creep suppression. ¹⁷ This $T_{\rm v}$ value is the target temperature for healing studies, which will be explored in the next section.

Photothermal Self-Healing. As mentioned, a key contribution of this work focuses on the photothermal self-healing of vitrimer films for coatings applications. Given the presence of AuNPs in our filler material, healing was performed using a 532 nm wavelength, continuous-wave laser (cf. Figures 1a and S11), as previously reported.²⁴ To photothermally heal a damaged vitrimer film, one reasonably assumes the following relevant experimental parameters: filler composition, filler concentration, the extent of damage, and laser dosage (power and exposure time).

For initial studies, minor damage was inflicted upon the sample surface (diamond-shaped indentations $\sim\!80~\mu\mathrm{m}$ diagonal length) using a microindenter. Subsequently, the damaged surface was exposed to a 532 nm laser at 10 mW power for varying time intervals until the damage was visually determined to be healed. For a direct comparison, the inflicted damage, laser power, and filler concentration were kept constant, while the filler composition and laser exposure time were varied (cf. Figure 4).

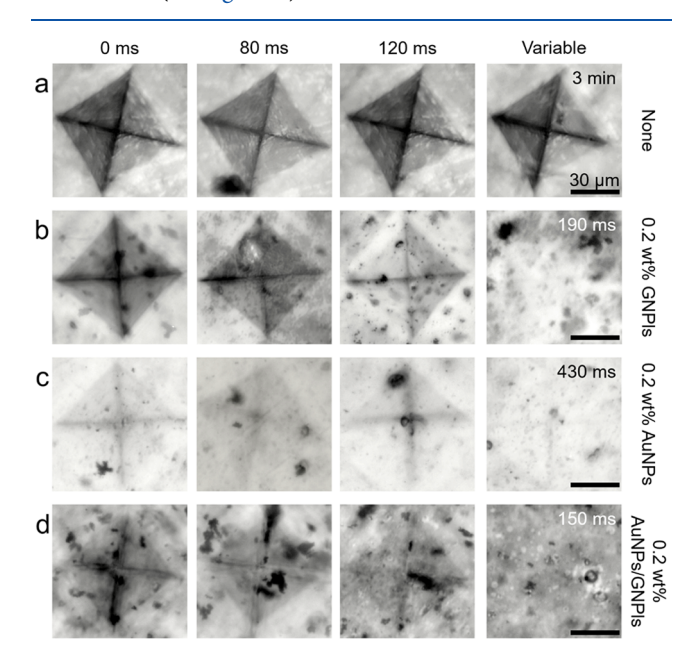


Figure 4. Nanoindentation experiments are performed where an indention is made on the surface of either a vitrimer film (a) or a vitrimer nanocomposite film (b-d) prior to laser exposure. The indented surface is exposed to a 532 nm laser at 10 mW power for times between 80 ms and 3 min. Optical microscopy is shown here to track sample healing with laser exposure. The filler concentration and composition are labeled on the right of each row, and the time of exposure is labeled on the top of each column. Clearly, the addition of filler increases the rate of heating and therefore sample healing.

Figure 4a clearly demonstrates that negligible healing is observed for neat vitrimer films, even with long laser irradiation times (up to 3 min). In contrast, vitrimer nanocomposite films with a 0.2 wt % concentration of nanofiller, visibly demonstrate complete healing at a variety of times (cf. Figure 4b,c, far right column). We postulate this healing is due to the photothermal effect caused by either the plasmonic resonance of the AuNPs, the light absorbance of the GNPls, or a combination of both. Unsurprisingly, the nanocomposite films containing AuNPs/GNPls heal in the shortest time of 150 ms compared to 190 and 430 ms for samples containing GNPls or AuNPs, respectively. This represents at least a 3-orders of magnitude improvement in the healing time between the AuNPs/GNPls and neat vitrimer. This increased healing response demonstrates a synergistic effect from combining both the absorbance of GNPls and the plasmonic resonance effect of the AuNPs. We should note that these ultrafast healing times outperform previous litera-

While nanoindentation is a useful demonstration for minor surface damage, it is critical to explore larger deformations, as one might find industrially (e.g., cracks). To this end, we

performed a series of experiments where a razor blade was used to manually cut the surface of the vitrimer and vitrimer nanocomposite films for laser-induced healing. We should note that unavoidable human error results in variable surface damage from sample to sample. However, the laser dosage was kept constant, and profilometry was performed on the sample surface before and after laser irradiation to track healing, as seen in Figure 5.

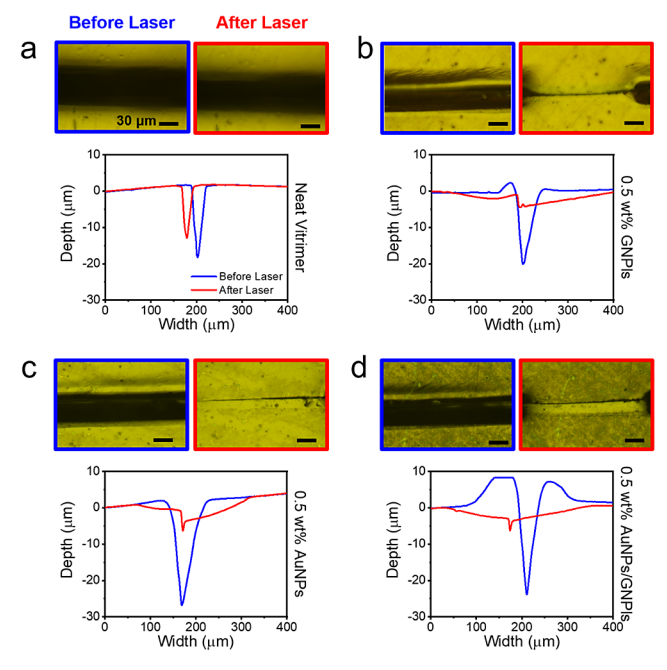


Figure 5. Images show the damaged surface of a vitrimer or vitrimer nanocomposite film: (a) neat vitrimer, (b) 0.5 wt % GNPIs, (c) 0.5 wt % AuNPs, and (d) 0.5 wt % AuNPs/GNPIs. The damage was manually inflicted with a razor blade (outlined in blue), the same surface is shown (outlined in red) after exposure to a 532 nm laser for 100 ms at a power of 20 W; all scale bars represent 30 μ m. Representative profilometry line scans are plotted for each sample showing the healing of each sample. The concentration and composition of filler in the material is listed on the right of each profilometry plot.

Comparing the images and graphs in Figure 5, it becomes clear that the vitrimer nanocomposites (cf. Figure 5b-d) vastly outperform the photothermally activated healing of a neat vitrimer film (cf. Figure 5a). This finding validates the need for filler addition, as previously demonstrated via nanoindentation for photothermal healing. Visually, all three nanocomposites show excellent recovery and healing after laser irradiation. To quantify these results, the profilometry scans of each cut before (blue) and after (red) laser exposure were analyzed and compared to quantify the amount of healing (cf. Figures 5,6), as detailed in the Supporting Information and displayed in Figures S12,S13. This analysis confirms that the highest performing filler material for all vitrimer nanocomposites tested here is AuNPs/GNPls; samples with a 0.5 wt % concentration of AuNPs/GNPIs yielded an average healing efficiency of 90.9% compared to neat vitrimer materials with an average healing efficiency of 11.5% (cf. Figure 7). Further information on healing efficiency is discussed in detail below.

While it is clear that AuNPs/GNPls are the prime choice for filler materials, it is worth considering the impact of filler concentration. It is reasonable to assume that an increase in

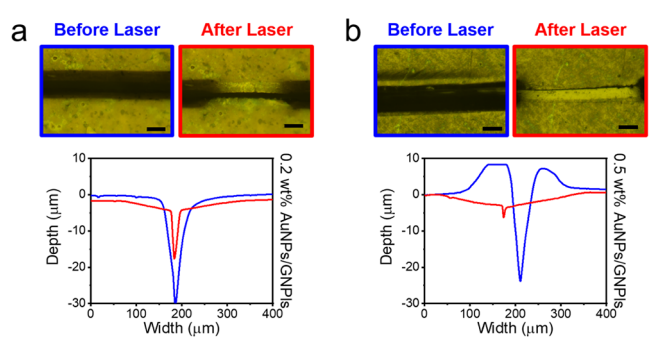


Figure 6. Images show the damaged surface of a vitrimer nanocomposite film (outlined in blue), where the damage was manually inflicted with a razor blade. The same surface is shown (outlined in red) after exposure to a 532 nm laser for 100 ms at a power of 20 mW; all scale bars represent 30 μ m. Vitrimer nanocomposites contain either 0.2 wt % AuNPs/GNPIs (a) or 0.5 wt % AuNPs/GNPIs (b). Representative profilometry line scans are plotted for each sample showing the healing of each sample.

filler concentration would lead to increased absorption, and therefore an increased photothermal healing response. For example, the samples for nanoindentation studies seen in Figure 4d exhibited healing in ~150 ms, while the scratched samples seen in Figure 5d with a higher filler concentration exhibited healing in ~100 ms. To quantify this impact of filler concentration, Figure 6 demonstrates visually and graphically an apparent increase in photothermally activated self-healing with an increase in filler concentration from 0.2 to 0.5 wt % AuNPs/GNPls.

As previously stated, the relevant experimental parameters for photothermally activated self-healing are filler composition, filler concentration, extent of damage, and laser dosage (power and exposure time). We have demonstrated qualitatively that the optimal filler material is AuNPs/GNPls, which is quantitatively confirmed in Figure 7a as measured via volume percent recovery (cf. eq S1). In addition, Figure 7b validates the unsurprising trend of increased photothermal healing with increasing filler concentration. Two varying surface damages have been successfully healed in the order of hundreds of microseconds: Microindents and surface scratches. Finally, we also explored the impact of laser power; we note that in this case, the laser irradiation time is kept constant at 100 ms, allowing for increasing dosage with increasing power. Figure 7c clearly indicates an increase in healing with an increased power. We should note that the power was not increased further due to the excellent healing associated with 30 mW of laser power coupled with concerns over damage to the sample surface, due to potential degradation or deformation from thermal expansion (cf. Figures S7 and S16).

Direct measurement of local temperature is ideal for further understanding fillers' influence during laser irradiation. Unfortunately, measuring such local phenomena is very challenging due to the laser spot size and equipment limitations. However, as the mechanism behind the film healing is the dynamic covalent bond exchange reaction in our vitrimer materials, it is reasonable to assume the local temperature exceeds the $T_{\rm v}$ value (i.e., 200–270 °C) for samples where healing is observed. To address this, molecular dynamics (MD) simulations²⁸ were performed to confirm the local temperature increase of our thin film.

MD simulation study in Figure 8 shows that the temperature of the AuNPs/GNPls filler rises rapidly at the start of the

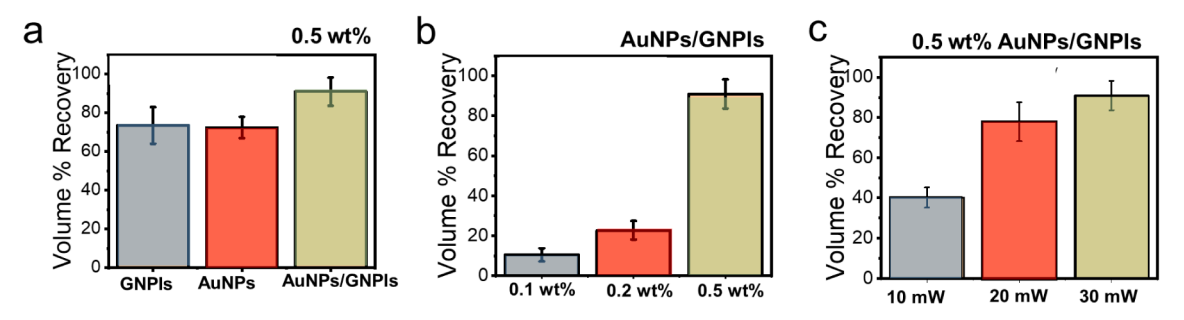


Figure 7. Histograms display the volume percent recovery as a function of either varying filler composition (a), filler concentration (b), or applied laser dosage (c). (a,b) Where the filler composition or concentration was varied, the applied laser conditions were held constant at a power of 20 mW and 100 ms of irradiation time. Error bars are calculated from the STDEV.S function in Excel, where sample sizes are the average of 10 lines per damaged site.

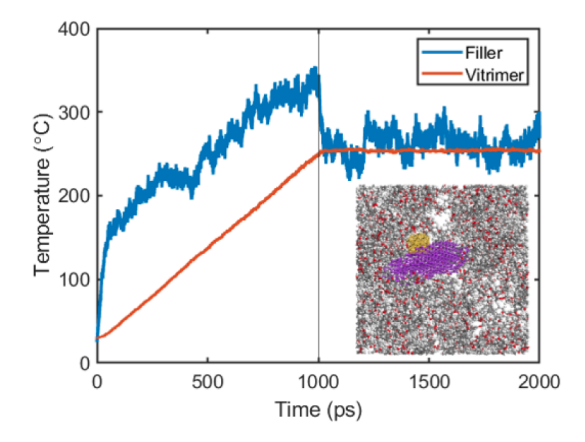


Figure 8. MD simulation displays the temperature change of the filler and vitrimers with the time increase. The inset is a schematic of the system. The golden ball represents the AuNP, the purple part shows bilayer graphene, and the rest is the vitrimer network.

heating process for a short period. Then, the heat conduction from the filler to the vitrimer matrix leads to a thermal equilibrium at the preset temperature of $T_{\rm v}$. Note that the filler reaches a peak temperature of 357 °C, which is much higher than $T_{\rm v}$. Such a high temperature softens the surrounding vitrimer chains and makes them kinetically more active. Despite the different spatial and temporal scales between simulation and experiment, the locally high temperature is evident. In other words, the vitrimers chains near the nanofillers are free to move and fill the gap in the damaged area so the bond exchange reactions, and thus self-healing, can occur.

Although Au and graphene are considered high thermal conductivity fillers, adding them does not show a noticeable increase in the thermal conductivity from that of the neat vitrimer, as confirmed by our transient thermal grating (TTG) measurements (Figures S14–S16). This is due to (1) the very low weight percentage of the fillers, (2) the size effect giving much lower thermal conductivity of the nanofillers than their bulk counterparts, and (3) the large thermal interface resistance between the filler and the vitrimer matrix. Our study suggests that the thermal conductivity increase is not necessary to obtain ultrafast self-healing because the nanofillers form many mini-hotspots where the temperature is much higher than the surroundings to facilitate the bond exchange in vitrimers and heat does not need to travel far to bring the overall equilibrium temperature to $T_{\rm v}$. This finding also

highlights the importance of having uniform nanofiller dispersion.

CONCLUSIONS

Herein, we demonstrated the ability to produce thin (\sim 100-300 μ m) vitrimer and vitrimer nanocomposite films with the potential for self-healing coatings. Three different filler compositions and concentrations were explored for vitrimer composite films and shown to outperform the self-healing capabilities of their neat vitrimer counterparts. Self-healing was achieved via exposure to a 532 nm laser, where the sample was placed on an adjustable stage for controlled movement. The optimal filler composition of the tested samples was a graphene nanoplatelet filled with gold nanoparticles (AuNPs/GNPls). The photothermally activated self-healing was demonstrated to increase with filler concentration and laser dosage (i.e., laser power and irradiation time). Of interest, all the healing times for samples with a 0.5 wt % filler concentration were ultrafast, exhibiting healing recovery of ≥70% within 100 ms. Two forms of sample damage were inflicted and successfully healed: Microindents and surface scratches. Ultrafast healing responses demonstrated by these films open up enormous potential for coatings and other industrial applications. Varying the composition of fillers, shape, size, and hierarchical architectures, optical and photon-phonon engineering is possible in these thin films, opening up a new avenue for sustainability in complex engineering devices and structures.²⁹

MATERIALS AND METHODS

Nanocomposite Film Synthesis. Bisphenol A diglycidyl ether (DGEBA), sebacic acid (SA), and the catalyst 1,5,7-triazabicyclo[4.4.0]dec-5-ene (TBD) were purchased from Sigma-Aldrich. Au(III) acetate (99.9%) was supplied by Alfa Aesar, and carbon graphite (Grade nano 24, Lot 2148) was provided by Asbury Carbons, Inc. All the materials and chemicals were used as received, unless otherwise stated.

The primary nanofillers studied herein were GNPIs and AuNPs/GNPIs; both materials were prepared as previously reported. 18

For nanocomposite film synthesis, the reaction was performed using an epoxy base (DGEBA) and the cross-linker (SA), in a 1:1 ratio mixture, with 5 mol % catalyst (TBD). Initially, the DGEBA precursor was shear mixed with the nanofillers (i.e., GNPIs, AuNPs, or AuNPs/GNPIs) at 3000 rpm for 10 min. The mixture was then placed in a bath sonicator for an additional 2 h, to ensure excellent dispersion. The mixture was then transferred to a 50 mL round-bottomed

flask and degassed under house vacuum (~100 psi) at 80 °C for 1 h to remove any trapped air. The temperature was then raised to 140 °C, and SA was introduced into the mixture before an additional 20 min of mixing under house vacuum. Subsequently, the 5 mol % catalyst (TBD) was added and stirred for 1 min prior to pour casting into a preheated and Frekote-coated Kapton sheet substrates. A metal shim with a thickness of 0.1 mm was placed between the two substrates to control the thickness of the film. The cast film was then placed in an oven to cure for 12 h at 180 °C. The fabrication process is illustrated in Figure S2. We should note that the neat vitrimer film production does not include the addition of fillers, and the synthesis procedure follows our previously reported methodologies. ^{23,30}

Characterization. Fourier Transform Infrared Spectroscopy (FTIR) was performed by using a Nicolet 380 FTIR.

All UV-vis spectra (both absorbance and extinction) were collected on a PerkinElmer Lambda UV-vis 950 spectrophotometer. The spectra were collected in triplicate in a range of 200–800 nm.

Tensile testing was performed on a TA Instruments DMA 850 instrument in a nitrogen environment. All the samples were cut into a dog bone shape (ASTM D628-14, Type V) prior to testing using a Keyence MDX 1520 laser cutter. The samples were equilibrated at $-10~^{\circ}\text{C}$ prior to testing at a ramp rate of 0.02 mm min⁻¹ until failure. A minimum of seven samples were tested to ensure statistical significance.

Scanning electron microscopy (SEM) was performed by using a field-emission SEM (Gemini 500) to characterize the morphology of the AuNPs/GNPIs. The images were taken at 15 keV, and the film was sputtered with a 10 nm coating of iridium prior to imaging.

All temperature sweep experiments were performed on a TA Instruments Discovery Hybrid rheometer (DHR-III) in tension mode under a nitrogen environment. The sample gap distance in all the cases was 15 mm, while the oscillating axial strain was 0.1% at a frequency of 1 Hz. The temperature was ramped from 20 to 100 °C at a temperature ramp rate of 5 °C min $^{-1}$. The $T_{\rm g}$ is recorded as the onset in the drop of the storage modulus or the maximum value of the tan (δ) .

All nonisothermal creep experiments were performed on a TA Instruments DHR-III in tension mode under a nitrogen environment. In all the cases, the applied engineering stress was 150 kPa at a temperature ramp rate of 5 °C min^{-1} from 20 to 350 °C.

All thermogravimetric analysis (TGA) experiments were performed on a TA Instruments TGA Q500 series. The samples were heated from room temperature to 1000 °C at a temperature ramp rate of 10 °C min⁻¹ in a nitrogen environment. The degradation temperature ($T_{5\%}$) is recorded as the temperature at which a sample has experienced a 5 wt % loss due to thermal degradation.

All differential scanning calorimetry (DSC) experiments were performed on a TA Instruments Discovery Series DSC 2500. The samples were heated and cooled in series between the temperatures of 10 and 200 °C at a temperature ramp rate of 5 °C min $^{-1}$. The $T_{\rm g}$ was recorded as the inflection point of the second heating curve.

A diamond-shaped indent (Vickers) with a diagonal length of 80 μ m was created on the film with a 300 μ m thickness using the MTS NanoXP nanoindentation system with a 0.5 N indentation load. The depths of the indents introduced to the

films at the same load were almost identical regardless of the filler types and concentration.

All photothermal self-healing studies were conducted using a 532 nm laser with varying power settings at a 20× magnification, infinity-corrected objective (Mitutoyo V80286315), similar to previously reported studies.²⁴ The laser $1/e^2$ beam radius was $44 \pm 0.2 \mu m$. Damaged samples were placed on the adjustable stage, directly under the microscope objective. The optical shutter controlled the exposure time of the damaged surface to the laser beam. Prior to sample irradiation, the laser power was determined using a power meter. Positioning of the laser beam on the sample was controlled using a two-axis translation stage, while the sample was simultaneously monitored using an in situ microscope. The exposure time was controlled using an optical shutter (Thorlabs SHB05T) and confirmed using a pick-off optic in conjunction with a photodiode (Thorlabs DET10A2) and an oscilloscope (Agilent Technologies DSO1012A).

Molecular Dynamics (MD) Simulation. In the MD simulations, we used an AuNP (1 nm diameter) connected with an oxygen atom on a $2.46 \times 2.56 \text{ nm}^2$ bilayer graphene as the AuNP/GNPI filler, and three 50-unit-length vitrimer chains as the vitrimer film to reflect the experimental samples. The structure was built in BIOVIA Materials Studio³¹ with periodic boundary conditions, as shown in the inset of Figure 8. We then performed the geometric optimization on the system within Material Studio using the Forcite module and polymer consistent force-field (PCFF), 32 ensuring the lacking Au-O bond coefficient was accurately replaced by the bond coefficient from universal force field (UFF).33 Later we used the LAMMPS³⁴ package to observe the temperature increase when the system is being heated. The system is first relaxed in isothermal-isobaric (NPT), canonical (NVT), and microcanonical (NVE) ensembles subsequently for 200 ps, and then the heat flux is added to the AuNP/GNPI filler within NVE ensembles for 1 ns to simulate the laser heating with power: $17.8e^{-3} \text{ kcal/mol/fs} \times (4.184 \text{ KJ/kcal}) \times (1e^{3} \text{ J/1 KJ}) \times (1e^{15} \text{ J/1 KJ})$ fs/1 s) = 7.45e¹⁶ J/s/mol. The amount of gold was $(4/3 \times \pi \times$ $(0.5e^{-9})^3 \text{ m}^3$ × 19.3e³ kg/m³ × (1e³ g/1 kg)/196.96657 g/ $mol = 5.13e^{-23}$ mol with the power on the AuNP: $7.45e^{16}$ J/s/ $mol \times 5.13e^{-23} mol = 3.82e^{-6} W$. The power of the heat flux is theoretically calculated via $p = mc\Delta T/t$, where m is the mass of the system, c is the heat capacity of the system, ΔT is the temperature difference between $T_{\rm v}$ (we chose 252 °C as a demo) and the room temperature, and t is the laser heating time (i.e., 1 ns in the simulation).

The heat capacity of the system is estimated via LAMMPS by fitting the total system energy change and the system temperature increase c = dE/dT. The estimated heat capacity of the system is 3.447×10^3 J/(kg·K), which is two times larger than the experimental heat capacity values of graphene, ¹⁹ SA, ³⁵ and DGEBA, ³⁶ and this derivation is common in the MD estimation. ³⁷

Transient Thermal Grating (TTG). TTG is an optical-based noncontact technique for measuring in-plane thermal diffusivity. In our TTG setup as shown in Figure S13, a picosecond Nd:YVO₄ laser (pulse duration 2 ps, wavelength λ_e = 517 nm, frequency 1 kHz, and energy 0.1 μ J per pulse) is used for excitation. ^{38,39} An electro-optically gated beam from a continuous-wave (CW) solid-state laser (wavelength λ_p = 532 nm, CW power 16 mW, chopped at 10% duty cycle with an effective power of 1.6 mW) is used as the probe beam. We used achromatic spherical lenses with focal distances f_1 = 15

cm and $f_2 = 10$ cm to focus the pump and probe beams onto the sample and generate thermal gratings. On the sample, the laser spot diameters are about 150 μ m for the excitation pulses, probe, and reference beams. The heterodyne phase is controlled with a motorized actuator by adjusting the angle of a glass plate. The diffracted signal combined with a reference beam, which is derived from the same source and attenuated by a neutral density filter (ND-3), is detected by a balanced amplified photodetector (bandwidth 45 MHz) whose output is recorded with an oscilloscope (4 GHz bandwidth). TTG measurements of transmission geometry are performed on nanocomposite thin films at the grating period L = 1.25 μ m. The example decay signal as shown in Figure S14 follows a single exponential decay curve with a decay time $\tau=1/(\alpha q^2)$, where α is the in-plane thermal diffusivity and $q = 2\pi/L$ is the grating wavevector. The measured α is plotted in Figure S15. The in-plane thermal conductivity is then obtained from the in-plane thermal diffusivity together with the density ρ and the specific heat capacity C_p as $k = \rho \times C_p \times \alpha$.

ASSOCIATED CONTENT

Supporting Information

Figure S1Figure S2Figure S3Figure S4Figure S5Figure S6Figure S7Figure S8Figure S9Figure S10Figure S11Figure S12Figure S13Figure S14Figure S15Figure S16Figure S17Figure S18The Supporting Information is available free of charge at https://pubs.acs.org/doi/10.1021/acsanm.4c02190

Scheme S1: Schematics showing (a) chemical structures of the reactants and catalyst, bisphenol A diglycidyl ether (DGEBA), sebacic Acid, and 1,5,7-triazabicyclo[4.4.0]dec-5-ene (TBD as a catalyst). (b) Chemical reactions showing acid and epoxy lead to an esterification reaction resulting in the growth of a polymeric chain (top) and transesterification reaction driven by the catalyst (bottom), the key mechanism for the dynamic reaction. Figure S1: FTIR confirms complete curing of the vitrimer material. Figure S2: Schematic diagrams depicting vitrimer synthesis where additional sonication and shear mixing are required for increased filler dispersion. Figure S3: Optical microscopy confirms increased filler dispersion with additional shear mixing and sonication via image analysis. Figure S4: HAADF-STEM and EDX confirm the presence of gold decorated on the graphene nanoplatelets. Figure S5. UV-visible spectroscopy (UV-vis) spectra show the evolution of transmission for three types of vitrimer nanocomposites at different weight percentages of filler content: (a) GNPIs, (b) AuNPs, and (c) AuNPs/GNPls. Figure S6: UV-vis is shown for all the vitrimer composites. Figure S7: TGA results are shown for all vitrimer nanocomposites. Figure S8: DSC results are shown for all the vitrimer nanocomposites. Tensile test results are shown for neat vitrimer and vitrimer nanocomposite films. Figure S9: Temperature sweep results from DMA are shown for all vitrimer composites. Figure S10: Nonisothermal creep is shown for increasing filler concentration. Figure S11: Schematic diagram depicting the laser apparatus utilized for all photothermal healing experiments. Figure S12: Profilometry scans are shown for vitrimer healing studies with a variety of filler compositions. Figure S13: Profilometry images and scans are shown to demonstrate the surface deformation

as a result of thermal expansion. Figure S14: Schematic diagram of TTG set up. Figure S15: Measured TTG signal for the 0.2 wt % GNPl vitrimer nanocomposite film. Figure S16: In-plane thermal diffusivity measured from TTG of different vitrimer nanocomposite films. Figure S17: Representative tensile stress—strain curve of thin vitrimer films showing the influence of filler and dispersion quality influencing the mechanical properties. Figure S18: Summary of the tensile testing data of neat vitrimer and composite: (a) Modulus (GPa) and strain at break (%), and (b) toughness (MJ/m³) (PDF)

AUTHOR INFORMATION

Corresponding Author

Dhriti Nepal — Materials and Manufacturing Directorate, Air Force Research Laboratory, Wright-Patterson Air Force Base, Ohio 45433, United States; orcid.org/0000-0002-0972-9960; Email: dhriti.nepal.1@us.af.mil

Authors

Yixin Ren — Materials and Manufacturing Directorate, Air Force Research Laboratory, Wright-Patterson Air Force Base, Ohio 45433, United States

Amber M. Hubbard — Materials and Manufacturing
Directorate, Air Force Research Laboratory, Wright-Patterson
Air Force Base, Ohio 45433, United States; National
Research Council Research Associate, Air Force Research
Laboratory, Wright-Patterson Air Force Base, Ohio 45433,
United States

Drake Austin — Materials and Manufacturing Directorate, Air Force Research Laboratory, Wright-Patterson Air Force Base, Ohio 45433, United States

Jinghang Dai — Sibley School of Mechanical and Aerospace Engineering, Cornell University, Ithaca, New York 14850, United States; orcid.org/0000-0003-0215-7602

Chen Li — Sibley School of Mechanical and Aerospace Engineering, Cornell University, Ithaca, New York 14850, United States

Renjiu Hu — Sibley School of Mechanical and Aerospace Engineering, Cornell University, Ithaca, New York 14850, United States; orcid.org/0000-0003-4651-3349

Peter Papaioannou — Materials and Manufacturing Directorate, Air Force Research Laboratory, Wright-Patterson Air Force Base, Ohio 45433, United States; Strategic Ohio Council for Higher Education (SOCHE) Program, Wright-Patterson Air Force Base, Ohio 45433, United States

Catalin R. Picu — Department of Mechanical, Aerospace, and Nuclear Engineering, Rensselaer Polytechnic Institute, Troy, New York 12180, United States; ⊙ orcid.org/0000-0001-8371-3564

Dominik Konkolewicz − Department of Chemistry and Biochemistry, Miami University, Oxford, Ohio 45056, United States; ocid.org/0000-0002-3828-5481

Alireza Sarvestani — Department of Mechanical Engineering, Mercer University, Macon, Georgia 31207, United States; oorcid.org/0000-0001-8762-7575

Nicholas Glavin — Materials and Manufacturing Directorate, Air Force Research Laboratory, Wright-Patterson Air Force Base, Ohio 45433, United States; orcid.org/0000-0002-9447-7509

Vikas Varshney – Materials and Manufacturing Directorate, Air Force Research Laboratory, Wright-Patterson Air Force

- Base, Ohio 45433, United States; o orcid.org/0000-0002-2613-458X
- Ajit K. Roy Materials and Manufacturing Directorate, Air Force Research Laboratory, Wright-Patterson Air Force Base, Ohio 45433, United States; orcid.org/0000-0002-3344-7437
- Zhiting Tian Sibley School of Mechanical and Aerospace Engineering, Cornell University, Ithaca, New York 14850, United States; oorcid.org/0000-0002-5098-7507

Complete contact information is available at: https://pubs.acs.org/10.1021/acsanm.4c02190

Author Contributions

OY.R. and A.M.H. are contributed equally to this work.; Y.R., A.M.H., V.V., A.K.R., and D.N. were involved in project conceptualization. Y.R., A.M.H., D.A., N.G., C.L., J.D., R.H., T.M., and Z.T. were involved in developing testing methodologies. Y.R., A.M.H., D.A., C.L., J.D., R.H., T.M., and P.P. were involved in the research investigation. Y.R. and A.M.H. wrote the initial draft of the article. All the authors were involved in the review and editing process. Z.T., C.R.P., D.K., A.S., V.V., A.K.R., and D.N. supervised the project.

Notes

The authors declare no competing financial interest.

ACKNOWLEDGMENTS

The authors thank Dr. Ming-Jen Pan, Capt. Derek Barbee, and Dr. Kenneth Caster of the Air Force Office of Scientific Research (AFOSR). This research was performed while A.M.H. held an NRC Research Associateship award at the Air Force Research Laboratory. This work was partially funded by Z.T.'s NSF CAREER Award (CBET1839384). N.G. and D.A. gratefully acknowledge support from the Asian Office of Aerospace Research and Development within the AFOSR grant #21IOA110. This manuscript is approved for public release from the Air Force Research Laboratory, Case No. AFRL-2023-6223.

REFERENCES

- (1) Jin, F.-L.; Li, X.; Park, S.-J. Synthesis and application of epoxy resins: A review. *J. Ind. Eng. Chem.* **2015**, 29, 1–11.
- (2) Zheng, J.; Png, Z. M.; Ng, S. H.; Tham, G. X.; Ye, E.; Goh, S. S.; Loh, X. J.; Li, Z. Vitrimers: Current research trends and their emerging applications. *Mater. Today* **2021**, *51*, 586–625.
- (3) Yang, Y.; Xu, Y.; Ji, Y.; Wei, Y. Functional epoxy vitrimers and composites. *Prog. Mater. Sci.* **2021**, *120*, 100710.
- (4) Zhao, X.; Long, Y.; Xu, S.; Liu, X.; Chen, L.; Wang, Y.-Z. Recovery of epoxy thermosets and their composites. *Mater. Today* 2023, 64, 72–97.
- (5) Li, B.; Cao, P.-F.; Saito, T.; Sokolov, A. P. Intrinsically Self-Healing Polymers: From Mechanistic Insight to Current Challenges. *Chem. Rev.* **2023**, *123* (2), 701–735.
- (6) Wang, S.; Li, B.; Zheng, J.; Surat'man, N. E. B.; Wu, J.; Wang, N.; Xu, X.; Zhu, J.; Loh, X. J.; Li, Z. Nanotechnology in Covalent Adaptable Networks: From Nanocomposites to Surface Patterning. ACS Mater. Lett. 2023, 5 (2), 608–628.
- (7) Rajaei, M.; Kim, N. K.; Bhattacharyya, D. Effects of heat-induced damage on impact performance of epoxy laminates with glass and flax fibres. *Compos. Struct.* **2018**, *185*, 515–523.
- (8) Schenk, V.; Labastie, K.; Destarac, M.; Olivier, P.; Guerre, M. Vitrimer composites: Current status and future challenges. *Mater. Adv.* **2022**, *3* (22), 8012–8029.

- (9) Zheng, J.; Png, Z. M.; Ng, S. H.; Tham, G. X.; Ye, E.; Goh, S. S.; Loh, X. J.; Li, Z. Vitrimers: Current research trends and their emerging applications. *Mater. Today* **2021**, *51*, 586–625.
- (10) Zhao, G.; Zhou, Y.; Wang, J.; Wu, Z.; Wang, H.; Chen, H. Self-Healing of Polarizing Films via the Synergy between Gold Nanorods and Vitrimer. *Adv. Mater.* **2019**, *31* (18), 1900363.
- (11) Ma, J.; Porath, L. E.; Haque, M. F.; Sett, S.; Rabbi, K. F.; Nam, S.; Miljkovic, N.; Evans, C. M. Ultra-thin self-healing vitrimer coatings for durable hydrophobicity. *Nat. Commun.* **2021**, *12* (1), 5210.
- (12) Yang, Z.; Wang, Q.; Wang, T. Dual-Triggered and Thermally Reconfigurable Shape Memory Graphene-Vitrimer Composites. ACS Appl. Mater. Interfaces 2016, 8, 21691–21699.
- (13) Wang, Z.; Li, Z.; Wei, Y.; Ji, Y. Gold Nanospheres Dispersed Light Responsive Epoxy Vitrimers. *Polymers* **2018**, *10* (1), 65.
- (14) Feng, Y.; Nie, Z.; Chen, J.; Gong, K.; Shan, Y.; Dong, F.; Fan, X.; Qi, S. Tuning the Dynamic Properties of Epoxy Vitrimers via Bioinspired Polymer—Nanoparticle Bond Dynamics. *ACS Macro Lett.* **2023**, *12* (9), 1201–1206.
- (15) Sasidharan, S.; Anand, A. Epoxy-Based Hybrid Structural Composites with Nanofillers: A Review. *Ind. Eng. Chem. Res.* **2020**, *59* (28), 12617–12631.
- (16) Nepal, D.; Haines, J.; Vaia, R. A. Polymer nanocomposites: 35 years on. MRS Bull. **2024**, 49 (3), 236–246.
- (17) Hubbard, A. M.; Ren, Y.; Papaioannou, P.; Sarvestani, A.; Picu, C. R.; Konkolewicz, D.; Roy, A. K.; Varshney, V.; Nepal, D. Vitrimer Composites: Understanding the Role of Filler in Vitrimer Applicability. *ACS Appl. Polym. Mater.* **2022**, *4* (9), 6374–6385.
- (18) Ren, Y.; Rao, R.; Bhusal, S.; Varshney, V.; Kedziora, G.; Wheeler, R.; Kang, Y.; Roy, A.; Nepal, D. Hierarchical Assembly of Gold Nanoparticles on Graphene Nanoplatelets by Spontaneous Reduction: Implications for Smart Composites and Biosensing. *ACS Appl. Nano Mater.* **2020**, *3* (9), 8753–8762.
- (19) Pop, E.; Varshney, V.; Roy, A. K. Thermal properties of graphene: Fundamentals and applications. *MRS Bull.* **2012**, *37* (12), 1273–1281.
- (20) Hubbard, A. M.; Ren, Y.; Sarvestani, A.; Konkolewicz, D.; Picu, C. R.; Roy, A. K.; Varshney, V.; Nepal, D. Recyclability of Vitrimer Materials: Impact of Catalyst and Processing Conditions. *ACS Omega* **2022**, *7* (33), 29125–29134.
- (21) Hubbard, A. M.; Ren, Y.; Sarvestani, A.; Picu, C. R.; Varshney, V.; Nepal, D. Thermomechanical analysis (TMA) of vitrimers. *Polym. Test.* **2023**, *118*, 107877.
- (22) Putnam-Neeb, A. A.; Kaiser, J. M.; Hubbard, A. M.; Street, D. P.; Dickerson, M. B.; Nepal, D.; Baldwin, L. A. Self-healing and polymer welding of soft and stiff epoxy thermosets via silanolates. *Adv. Compos. Hybrid Mater.* **2022**, *5* (4), 3068–3080.
- (23) Hubbard, A. M.; Ren, Y.; Konkolewicz, D.; Sarvestani, A.; Picu, C. R.; Kedziora, G. S.; Roy, A.; Varshney, V.; Nepal, D. Vitrimer Transition Temperature Identification: Coupling Various Thermomechanical Methodologies. *ACS Appl. Polym. Mater.* **2021**, 3 (4), 1756–1766.
- (24) Austin, D.; Gliebe, K.; Muratore, C.; Boyer, B.; Fisher, T. S.; Beagle, L. K.; Benton, A.; Look, P.; Moore, D.; Ringe, E.; et al. Laser writing of electronic circuitry in thin film molybdenum disulfide: A transformative manufacturing approach. *Mater. Today* **2021**, *43*, 17–26
- (25) Yang, L.; Li, L.; Lu, J.; Lin, B.; Fu, L.; Xu, C. Flexible Photothermal Materials with Controllable Accurate Healing and Reversible Adhesive Abilities. *Macromolecules* **2023**, *56* (8), 3004–3014
- (26) Cho, Y. J.; Kong, L.; Islam, R.; Nie, M.; Zhou, W.; Lu, K. Photothermal self-healing of gold nanoparticle—polystyrene hybrids. *Nanoscale* **2020**, *12* (40), 20726–20736.
- (27) Chen, M.; Chen, B.; Li, D.; Luo, W.; Zhang, H. Development of a Multistimulus Response Silicon-Bridged/Fe3O4 Epoxy Vitrimer: Controllable Welding, Crack Healing, and Shape Memory. *ACS Appl. Polym. Mater.* **2023**, 5 (12), 9931–9939.

- (28) Ma, H.; Babaei, H.; Tian, Z. The importance of van der Waals interactions to thermal transport in Graphene-C60 heterostructures. *Carbon* **2019**, *148*, 196–203.
- (29) Ling, Z.; Chen, J.; Li, S.; Lu, H.; Du, J.; Liu, Z.; Qiu, J. A multiband stealth and anti-interference superspeed light-guided swimming robot based on multiscale bicontinuous three-dimensional network. *Chem. Eng. J.* **2024**, 485, 150094.
- (30) Hubbard, A. M.; Ren, Y.; Picu, C. R.; Sarvestani, A.; Konkolewicz, D.; Roy, A. K.; Varshney, V.; Nepal, D. Creep Mechanics of Epoxy Vitrimer Materials. *ACS Appl. Polym. Mater.* **2022**, *4* (6), 4254–4263.
- (31) BIOVIA, Dassault Systèmes, Material Studio; Dassault Systèmes: San Diego, 2019.
- (32) Plimpton, S. Fast Parallel Algorithms for Short-Range Molecular Dynamics. *J. Comput. Phys.* **1995**, *117* (1), 1–19.
- (33) Rappe, A. K.; Casewit, C. J.; Colwell, K. S.; Goddard, W. A., III; Skiff, W. M. UFF, a full periodic table force field for molecular mechanics and molecular dynamics simulations. *J. Am. Chem. Soc.* **1992**, *114* (25), 10024–10035.
- (34) Thompson, A. P.; Aktulga, H. M.; Berger, R.; Bolintineanu, D. S.; Brown, W. M.; Crozier, P. S.; In't Veld, P. J.; Kohlmeyer, A.; Moore, S. G.; Nguyen, T. D.; et al. LAMMPS a flexible simulation tool for particle-based materials modeling at the atomic, meso, and continuum scales. *Comput. Phys. Commun.* **2022**, 271, 108171.
- (35) Bloxham, J. C.; Hill, D.; Knotts, T. A., IV; Giles, N. F.; Wilding, W. V. Liquid Heat Capacity Measurements of the Linear Dicarboxylic Acid Family via Modulated Differential Scanning Calorimetry. *J. Chem. Eng. Data* **2020**, 65 (2), 591–597.
- (36) Djemour, A.; Sanctuary, R.; Baller, J. Mobility restrictions and glass transition behaviour of an epoxy resin under confinement. *Soft Matter.* **2015**, *11* (13), 2683–2690.
- (37) Bhowmik, R.; Sihn, S.; Varshney, V.; Roy, A. K.; Vernon, J. P. Calculation of specific heat of polymers using molecular dynamics simulations. *Polymer* **2019**, *167*, 176–181.
- (38) Li, C.; Ma, Y.; Tian, Z. Thermal Switching of Thermoresponsive Polymer Aqueous Solutions. ACS Macro Lett. 2018, 7, 53.
- (39) Li, C.; Ma, Ĥ.; Li, T.; Dai, J.; Rasel, M. A. J.; Mattoni, A.; Alatas, A.; Thomas, M. G.; Rouse, Z. W.; Shragai, A.; Baker, S. P.; Ramshaw, B. J.; Feser, J. P.; Mitzi, D. B.; Tian, Z. Remarkably Weak Anisotropy in Thermal Conductivity of Two-Dimensional Hybrid Perovskite Butylammonium Lead Iodide Crystals. *Nano Lett.* **2021**, 21, 3708–3714.